Dissociation of value and confidence signals in the orbitofrontal cortex during decision-making: an intracerebral electrophysiology study in humans

Thelma Landron, Alizée Lopez-Persem, Philippe Domenech, Katia Lehongre, Vincent Navarro, Sylvain Rheims, Philippe Kahane, Julien Bastin, Mathias Pessiglione

Title:

Dissociation of value and confidence signals in the orbitofrontal cortex during decision-making: an intracerebral electrophysiology study in humans

Abbreviated title:

iEEG signals in the OFC during value-based choice

Authors and affiliations:

Thelma Landron[1], Alizée Lopez-Persem[1], Philippe Domenech[1], Katia Lehongre[1], Vincent Navarro[1,2], Sylvain Rheims[3,4], Philippe Kahane[5,6], Julien Bastin[5] and Mathias Pessiglione[1]

[1] Paris Brain Institute (ICM), Sorbonne Université, Inserm UMR1127, CNRS UMR 7225, 75013 Paris, France

[2] Epilepsy Unit, Pitié-Salpêtrière Hospital, Assistance Publique - Hôpitaux de Paris, Sorbonne Université, 75013 Paris, France

[3] Lyon Neuroscience Research Center, INSERM U1028, CNRS UMR5292, Université Claude Bernard Lyon 1, 69500 Bron, France

[4] Department of Functional Neurology and Epileptology, Hospices Civils de Lyon, Université Claude Bernard Lyon 1, 69500 Bron, France

[5] Grenoble Institute of Neuroscience, INSERM U1216, Université Grenoble Alpes, 38700 La Tronche, France

[6] Centre Hospitalo-Universitaire Grenoble Alpes, Université Grenoble Alpes, 38700 La Tronche, France

Corresponding author: Mathias Pessiglione (mathias.pessiglione@gmail.com)

Number of pages: 36

Number of figures: 7; **tables:** 0; **extended figures:** 3

Number of words for abstract: 240; **introduction:** 650; **and discussion:** 1487

Conflict of interest statement: The authors declare no competing financial interests.

Acknowledgments: We would like to thank Jean Daunizeau and Sébastien Bouret for insightful comments. We are also grateful to Laurence Hunt for providing the code of his neural network model. TL was supported by the École de l'INSERM Liliane Bettencourt and funded by the Fondation pour la Recherche Médicale (ECO201906008985, FDT202204014807). The study was funded by the Investissements d'Avenir program (ANR-10-IBHU-0003).

Abstract

Some decisions, such as selecting a food item in a novel menu, are not based on rational norms, or on trained habits, but on subjective preferences. How the human brain makes these preference-based decisions is still debated in cognitive neuroscience. Classical models focus on the comparison mechanism that achieves the selection of the option with best expected value. Recent models suggest that estimates of option values are refined until reaching sufficient confidence in the considered choice. Neuroimaging studies in humans and electrophysiology studies in animals have gathered evidence that value and confidence estimates are both represented in medial and lateral regions of the orbitofrontal cortex (OFC). Here, we took advantage of electrodes implanted within the OFC of human patients with pharmaco-resistant epilepsy (14 women, 12 men) to investigate whether value and confidence estimates can be dissociated in electrophysiology activity recorded during preference-based binary decisions. The overall value (liking ratings summed over options) and choice confidence (selection probability of the chosen option) were identified in low-frequency (4-8 Hz) OFC activity. These value and confidence signals were time-locked to the decision, showed opposite signs of correlation and were recorded in separate sites. This pattern of results is not consistent with the simulations of an attractor neural network model implementing a comparison of option values. However, it is compatible with the notion of a neural network generating sparse representations of option values and choice confidence estimates, based on which decisions can be made.

Significance statement

The orbitofrontal cortex (OFC) is known to play a critical role in decisions based on subjective preferences, such as choosing between food items in a menu. However, the information provided by the human OFC has remained elusive, due to limitations of neuroimaging techniques. Here, taking advantage of electrodes implanted in patients for clinical purposes, we present a rare dataset of electrophysiological activity recorded during preference-based decisions. Our analyses suggest that the OFC signals two distinct constructs on which decisions could be based: the subjective values of available options and the confidence in the intended choice.

Introduction

Cheese or dessert? Bowling or dancing? Art or science? Many choices, from mundane activities to career paths, are based on subjective preferences rather than normative principles. How the human brain makes these so-called preference-based decisions is a central question in cognitive neuroscience.

At the computational level, the decision process is traditionally decomposed into 1) valuation of choice options, and 2) selection of the best option. Valuation is understood as an integration over attributes of choice options, and selection reduced to a comparison between option values (Glimcher & Rustichini, 2004; Rangel et al., 2008; Padoa-Schioppa, 2011). However, these simple computational accounts only solve the problem of which option should be selected, not when the decision should be made. To address that issue, evidence accumulation models were borrowed from theories of perceptual decision and applied to preference-based decisions (Krajbich et al., 2010; Philiastides et al., 2010). These models assume that the relative preference for a given option is accumulated over time, until it reaches a bound that triggers the choice. Although passive accumulation makes sense for perceptual evidence, which is a noisy indicator of some external feature (such as light), it cannot capture the formation of subjective preference, which must be internally constructed from information stored in memory. For this reason, accumulation models were reframed as a tradeoff between the time invested in deliberation and the confidence gained in preference estimation (Lee & Daunizeau, 2021; Bénon et al., 2024). In this perspective, the brain would need to estimate both the value of choice options and the confidence in the forthcoming decision.

At the neural level, value and confidence estimates were both linked to activity in the orbitofrontal cortex (OFC). In humans, fMRI studies identified the ventromedial prefrontal cortex (vmPFC) as a key valuation node, notably during liking rating or even during distractive tasks (Lebreton et al., 2009; Levy et al., 2011; Shenhav & Karmarkar, 2019; Suzuki et al., 2017). In non-human primates, single-unit electrophysiology studies found value signals in both the vmPFC and the lateral OFC (Tremblay & Schultz, 1999; Padoa-Schioppa & Assad, 2006; Strait et al., 2014; Abitbol et al., 2015). Bridging across techniques and species, we previously recorded intracerebral EEG (iEEG) activity from electrodes implanted in human patients with pharmaco-resistant epilepsy, and found evidence for value signals during liking rating, in both the vmPFC and the lOFC, which we designate together by the global

label ‘OFC’ (Lopez-Persem et al., 2020). Confidence was also related to vmPFC activity by human fMRI studies, during both perceptual decisions (Bang & Fleming, 2018; Gherman & Philiastides, 2018; Rouault et al., 2023) and preference-based decisions (De Martino et al., 2013).

However, the dissociation of value and confidence signals is not straightforward. It is easier during rating tasks, in which confidence varies as a quadratic (U-shaped) function of value (Lebreton et al., 2015; De Martino et al., 2017). It is trickier during choice tasks, in which OFC activity typically reflects the difference between chosen and unchosen option values (Gläscher et al., 2009; Chau et al., 2014; Gherman & Philiastides, 2018). Despite being related to value comparison, this difference signal is close to a notion of confidence, defined as the subjective probability of making the right choice. A seminal MEG study (Hunt et al., 2012) concluded that the vmPFC reflects first the sum and then the difference of option values. Using fMRI, we generalized this distinction to identify brain regions signaling value and confidence across rating and choice tasks (Clairis & Pessiglione, 2022). There was an overlap, with value being represented in more posteroventral, and confidence in more anterodorsal parts of the medial prefrontal cortex. Thus, fMRI recordings suggest a spatial gradient, whereas MEG recordings suggest a temporal dissociation between value and confidence signals.

Leveraging iEEG spatial and temporal resolution, our aims here were to test whether value and confidence signals, recorded within the OFC while patients performed preference-based decisions, could be dissociated in space and/or time.

Methods

Participants

35 participants (37.9 ± 10.7 years, 21 females) were informed and gave written consent to their inclusion in the study. Participants were the same as described in our previous study (Lopez-Persem et al., 2020). They were patients with pharmaco-resistant focal epilepsy who were stereotactically implanted with multilead depth electrodes as part of a pre-resection procedure. Surgical implantations and iEEG recordings took place in three different epilepsy departments: Lyon (n = 18), Grenoble (n = 6) and Paris (n = 11). Procedures were approved by French Ethics Committee (CPP 09-CHUG-12, study 0907 for Lyon and Grenoble; CPP Paris VI, Pitié-Salpêtrière Hospital, INSERM C11-16 for Paris).

Recordings

Intracerebral activity was recorded in patients after the stereotactical implantation of multilead depth electrodes (as described in Lachaux et al., 2003; Lopez-Persem et al., 2020). In Grenoble and Lyon, 12 to 18 semi-rigid 0.8-mm-wide electrodes, with 6 to 18 leads of 2 mm positioned 1.5-mm apart (Dixi), were implanted in each patient, depending on the targeted region. Anatomical localization of electrode contacts was determined by positioning individual stereotactic scheme in the proportional atlas of Talairach and Tournoux (Talairach & Tournoux, 1988), after adjustment for brain size. Brain activity was recorded using an audio-video-EEG monitoring system (Micromed), equipped with 128 or 256 depth-EEG channels sampled at 512 Hz (0.1 to 200 Hz bandwidth). A contact located in the white matter served as a reference.

In Paris, brain activity was recorded using a Neuralynx system (ATLAS, Neuralynx, Inc.), via 4-to-12 platinum contact, 1-mm-wide, 1.6-mm-long, nickel-chromium wired electrodes (AdTech). The contacts were anatomically localized on the basis of post-implant CT scans coregistered to pre-implant 1.5-T MR scans. A bandpass filter (0.1 Hz to 1,000 Hz) was used and the least active electrode (in the white matter whenever possible) was set as reference. Anatomical localization in the MNI space was automatically recovered using the Epiloc toolbox (v.V1, STIM engineering facility at the Paris Brain Institute; García-Pérez et al., 2015).

Before preprocessing, all contacts were re-referenced to their nearest neighbor on the same electrode, yielding bipolar derivations for signal analysis.

Experimental tasks

Participants completed two tasks: a likeability rating task in which they rated how much they would like to receive each of the items that were presented on screen sequentially, and a binary choice task in which they chose between two items presented simultaneously the one they would prefer to receive. The results related to the rating task have already been reported (Lopez-Persem et al., 2020).

Behavioral tasks used in Paris were programmed on a PC using Matlab 2013 and the Cogent 2000 (Wellcome Department of Imaging Neuroscience, London, UK) library of Matlab functions for stimulus presentation. Behavioral tasks used in Lyon and Grenoble were programmed using Presentation software (v.16.5, Neurobehavioral Systems). A set of 60 food items was used in Paris (for 60 rating and 60 choice trials), and 120 food items in Lyon and Grenoble (for 120 rating and 120 choice trials). All trials started with a fixation cross lasting for 1,500 ± 500 ms in rating tasks and for 2,500 ± 500 ms in choice tasks. There was no time limit for making the response (rating or choice).

In the likeability rating task (Fig. 1A, top panel), participants rated how much they liked food items, presented one by one in a random order, on a 21-step scale (from –10 to 10). For each rating, the initial position of the cursor was randomized. Using their right hand, participants could move it by pressing the left and right arrows on the keyboard and then validate its final position by pressing the space bar.

In the binary choice task (Fig. 1A, bottom panel), participants expressed their preference between food items presented two by two. Likeability ratings were used to pair the food items such that in half the trials, the mean option value was varied while the distance was kept constant, and vice versa for the other half. Mean value is the average of likeability ratings and distance the unsigned difference between the two. The position of food items within a pair (left or right of fixation cross), and the presentation order of option pairs within a block (constant-mean or constant-distance), were pseudo-randomized. Participants indicated which item they preferred by pressing the left or right arrow of the keyboard.

Behavioral data analysis.

Only trials with 0.1 < RT < 10 s were included in the analysis (15 trials removed out of 2398 trials in total). Likeability ratings (z-scored) were taken as option values for the analysis of binary choices. We first tested the psychometric properties of choice behavior to check that participants had understood the tasks, with 1) a logistic regression of choice against the signed difference between option values and (2) a linear regression of RT against the distance (unsigned difference) between option values. Unless otherwise specified, all regressions were conducted at the individual level and tested for significance at the group level, using two-tailed, paired t-tests (random-effect analysis). All statistical analyses were performed using Matlab Statistical Toolbox (Matlab R2020a, The MathWorks, Inc.).

ROI definition.

The Automated Anatomical Labelling (AAL; Tzourio-Mazoyer et al., 2002) atlas was restructured as explained in our previous study (Lopez-Persem et al., 2020). The vmPFC ROI was defined by merging the regions labeled as gyrus rectus and frontal medial orbital, and the lOFC ROI by merging the frontal superior orbital and the frontal middle orbital regions. Coordinates of recording sites were calculated by averaging the MNI coordinates of the two contacts composing the bipolar derivation. The original dataset included a total of 4,273 recording sites in 35 participants. Among the 3,440 remaining recording sites after removal of those with low-quality signal, 204 sites were located within one of our OFC ROI (vmPFC + lOFC; Fig. 2).

Electrophysiological signal processing.

Recorded iEEG activity was analyzed using the FieldTrip Matlab toolbox for electrophysiological analysis (http://www.ru.nl/neuroimaging/fieldtrip; Oostenveld et al., 2011) as well as homemade Matlab scripts. Derivations were computed between adjacent recording sites, from a same electrode, yielding a bipolar montage. Because contributions from non-local assemblies were cancelled out, the signal was considered as originating from a cortical volume centered in-between the two contacts, referred to as

182 the recording site (Jerbi et al., 2009). The signal was band-pass filtered (2-200 Hz) and the 50-Hz line
183 noise was notch-filtered out.
184 Next, iEEG signal was decomposed using a 'multitapering' time-frequency transform (Slepian
185 tapers, lower frequency range: 2-32 Hz, 6 cycles and 3 tapers per window; higher frequency range: 32-
186 200 Hz, fixed time windows of 240 ms, 4-31 tapers per window). To enable more precise power
187 estimation, smoothing was adaptively increased across frequencies by using a constant number of cycles
188 across frequencies up to 32 Hz (hence a time window that expands when frequency increases), and a
189 fixed time window with an increasing number of tapers above 32 Hz.
190 For the frequency-specific analysis, continuous iEEG signals were first bandpass filtered in sub-
191 bands of 1-Hz width using a zero-phase shift, noncausal, finite impulse filter with 0.5-Hz roll-off. The
192 envelope of each sub-band was then computed using the standard Hilbert transform. The resulting
193 envelope signal, i.e., time-varying amplitude, was down-sampled to 64 Hz (duration of a time sample:
194 15.625 ms), and normalized (divided by its mean across the entire recording session and multiplied by
195 100). A single timeseries was then estimated by averaging envelopes across sub-bands. Of note, the
196 mean value of timeseries over the entire session is 100 for each band, by construction. This procedure
197 was meant to counteract the bias favoring higher frequencies induced by the 1/f drop-off in amplitude.
198
199 ***Electrophysiological data analysis.***
200 Analyses of iEEG activity were first focused on the standard θ band (4-8 Hz), because it matches with
201 both the low-frequency range in which value and confidence signals were initially observed (Hunt et
202 al., 2012) and with the main cluster of choice-evoked increase in power (see Fig. 3A). Frequency-
203 specific time series of iEEG activity recorded from each site were epoched on trial durations with two
204 possible time-locking: either to stimulus onset (option display) or response selection (button press). For
205 each time point, the signal was then regressed across trials against a general linear model (GLM):

$$signal = \beta_0 + \beta_1 \cdot baseline + \beta_2 \cdot Val + \beta_3 \cdot Conf + \beta_4 \cdot \#trial + \beta_5 \cdot RT + \varepsilon \quad \text{(Eq. 1)}$$

206 where baseline is the mean signal over the [–1, 0]-s pre-stimulus time window, Val the sum of chosen
207 and unchosen option values, Conf the probability that the chosen option is the best (provided by the

logistic function of chosen-minus-unchosen option value difference), #trial the trial number, and RT the response time. All regressors were serially orthogonalized (from left to right).

Statistical significance of regression estimates was computed across recording sites (n = 204), using two-tailed one-sample t-tests. Two corrections for testing multiple time/frequency points were implemented. The first is Bonferroni correction, which consists in dividing the significance threshold by the number of data points. The second correction integrates statistical dependencies across frequencies and time points, which were estimated based on random-field theory, using the VBA_toolbox (available at http://mbb-team.github.io/VBA-toolbox/; Daunizeau et al., 2014).

Several control analyses were conducted to assess the solidity of the findings. To ensure that results were not driven by particular individuals, an intercept per participant was added as a random factor in a mixed-effect GLM (using Matlab function *fitglme*) and residual regression estimates within a peri-response [–0.5 s, 0.5 s] time window were tested against zero. Another control analysis was run to address the issue that Val and Conf constructs are partially correlated, as they share a common term (the chosen option value). The regressors were orthogonalized in the GLM but this orthogonalization itself could generate spurious correlations. To mitigate potential artifacts due to the orthogonalization of regressors in the main GLM (Eq. 1), the analysis was repeated with a GLM that included only Val (without Conf) or only Conf (without Val):

$$signal = \beta_0 + \beta_1 \cdot baseline + \beta_2 \cdot Val + \beta_3 \cdot \#trial + \beta_4 \cdot RT + \varepsilon \quad \text{(Eq. 2)}$$

$$signal = \beta_0 + \beta_1 \cdot baseline + \beta_2 \cdot Conf + \beta_3 \cdot \#trial + \beta_4 \cdot RT + \varepsilon \quad \text{(Eq. 3)}$$

Another issue is that the GLM approach would fail to detect correlates of Val and Conf if the sign of regression estimates is not consistent across electrodes. The GLM analysis was complemented by an estimation of explained variance, which is agnostic about the sign of the association between the signal and the variable of interest, as is classically done in iEEG studies (e.g., Saez et al., 2018). Because there was some correlation between Val and Conf, the analysis was conducted for each variable in the null space of the other variable (i.e., after removing the variance explained by the other variable). The direction of the regression was reversed: Val and Conf (corrected for the other variable) were regressed against the signal (also corrected for the other variable). Regression estimates were then used to generate the Val and Conf predicted by the signal, which were correlated to the observed Val and Conf. The

variance in Val or Conf explained by the signal is simply the square of the correlation coefficient. Statistical significance was then assessed by comparing the obtained variance to the null, estimated using 200 random permutations of trial numbers.

We also investigated the extent to which Val and Conf signals are originating from the same recording sites. To that end, we computed a single regression estimate per site by fitting the main Val/Conf GLM (Eq. 1) to the mean θ signal over the peri-response [–0.5 s, 0.5 s] time period. The correlation of the resulting Val and Conf regression estimates was tested across recording sites using Pearson's coefficient. Significance at the site level was assessed by comparing regression estimates against zero using a t-test. This test served to identify the sites exhibiting a significant correlation with either Val or Conf, or both. The figures that display the localization of Val and Conf signals on frontal and sagittal slices of the anatomical MNI brain template were made using the FSL function *fslmaths* (to create the anatomical mask of the recording sites; Jenkinson et al., 2012) and MRIcroGL (to superimpose the anatomical mask onto the MNI template; www.nitrc.org/projects/mricrogl).

The spatial distribution of Val and Conf signals within the OFC was investigated to test for a dissociation between vmPFC and lOFC regions (along the mediolateral x-axis), and for a posteroventral-to anterodorsal gradient (along the yz axis) that was previously observed for value and confidence in the medial prefrontal cortex (De Martino et al., 2017; Clairis & Pessiglione, 2022). Peri-response Val and Conf signals (i.e., regression estimates across trials) were regressed against MNI coordinates of each axis separately, as well as the composite yz-axis:

Medial-lateral $$\beta_{Val/Conf} = \beta_0 + \beta_1 \cdot |x| + \varepsilon \quad \text{(Eq. 4)}$$

Posterior-anterior $$\beta_{Val/Conf} = \beta_0 + \beta_1 \cdot y + \varepsilon \quad \text{(Eq. 5)}$$

Ventral-dorsal $$\beta_{Val/Conf} = \beta_0 + \beta_1 \cdot z + \varepsilon \quad \text{(Eq. 6)}$$

Posteroventral-anterodorsal $$\beta_{Conf} - \beta_{Val} = \beta_0 + \beta_1 \cdot \sqrt{y^2 + z^2} + \varepsilon \quad \text{(Eq. 7)}$$

To better specify Val and Conf signals, the significant recording sites driving the main result (negative correlation with Val and positive correlation with Conf) were selected and their θ activity was regressed against additional GLMs including either chosen and unchosen option values (Ch and Unch) or reaction time (RT):

$$signal = \beta_0 + \beta_1 \cdot baseline + \beta_2 \cdot Ch + \beta_3 \cdot Unch + \beta_4 \cdot \#trial + \beta_5 \cdot RT + \varepsilon \quad \text{(Eq. 8)}$$

$$signal = \beta_0 + \beta_1 \cdot baseline + \beta_2 \cdot RT + \varepsilon \quad \text{(Eq. 9)}$$

Note that the unchosen value regressor (Unch) was not orthogonalized to the chosen value regressor (Ch) in Eq. 8.

Additionally, the mean θ activity over the peri-response [–0.5 s, 0.5 s] time period was compared between trials presenting easy vs. hard choices (sorted by median-split of distance between option values) and between trials ending with consistent vs. inconsistent choice (consistent meaning that the best-rated option was selected).

Value-comparison model simulations.

We simulated the choices that an attractor network model would make when offered the same options as our participants. The model used to simulate the value-comparison process is a mean-field reduction (detailed in Wong & Wang, 2006) of a spiking neuronal network (described in Wang, 2002) that was adapted to the case of economic binary choice (by Hunt et al., 2012). The network is reduced to two units, each receiving external input currents proportional to the value of one specific option, as well as noisy background input that resembles endogenous noise in the cortex. Synaptic connections include an excitatory recurrent coupling onto each unit and an effective inhibitory coupling to the other unit. The firing rate of each unit is then calculated as a monotonic function of the total synaptic input (integrating external and internal currents). We kept the specifics of the script kindly provided by Laurence Hunt, except for adjustments to our task and participants:

1) The number of simulated datasets was increased to 26 (number of participants included in the present study), and the number of trials to 60 or 120 (depending on the version of the task that was performed).
2) Actual likeability ratings were used for option values, after normalization to match the range of values used in the initial simulations (Hunt et al., 2012).
3) The duration was increased ([–1, 5] s, stimulus-locked) to ensure that a decision was reached. Stimulation (input values) was suppressed 1 s after it started, to match the $RT_{95\%}$ of participants.

4) The input strength parameter was adjusted ($k_{opt} = 0.225$) to match the average choice consistency (i.e., the proportion of trials in which the best-rated option is selected) observed across our participants.

Simulations were done separately for each participant and were then averaged across participants. We then added a couple of extra-simulations. First, we time-locked the activity to the decision, defined when one of the units reached a fixed threshold of 30 Hz (as was done in Hunt et al., 2012). The total activity of the network (synaptic current summed over the two units) was then regressed across trials against the same GLM as done with iEEG activity (with left-to-right serial orthogonalization):

$$activity = \beta_0 + \beta_1 \cdot Val + \beta_2 \cdot Conf + \beta_3 \cdot \#trial + \beta_4 \cdot RT + \varepsilon \qquad \text{(Eq. 10)}$$

Note that we have not decomposed the simulated activity into frequency bands, because specific oscillations can be arbitrarily generated by changing the time constants and noise parameters in the model.

Results

Choice behavior

For our purposes, we restricted our sample to the subgroup of patients with electrical contacts in the OFC (n = 26, age = 37.2 ± 10.2 years, 14 females), who performed both likeability rating and binary choice tasks (Fig. 1A). Likeability ratings were used as proxies for the values assigned to options in the analysis of choice behavior. Choice rate (frequency of left choice) was significantly related to decision value (difference between left and right option value) in a logistic regression model ($\beta_{Vl-Vr} = 1.89 \pm 0.21$, $t_{Vl-Vr}(26) = 9.07$, $p_{Vl-Vr} = 2.23 \cdot 10^{-9}$; Fig. 1B, top panel). Choice reaction time (RT) was significantly related to choice easiness (i.e., negatively correlated to the distance between option values) in a linear regression model ($\beta_{|Vl-Vr|} = -0.21 \pm 0.04$, $t_{|Vl-Vr|}(26) = -5.47$, $p_{|Vl-Vr|} = 1.12 \cdot 10^{-5}$; Fig. 1B, bottom panel). Thus, standard psychometric measures confirmed that patients were making decisions based on their subjective preferences.

We also checked the psychometric properties of our two key constructs for value and confidence, noted Val (for the sum of option values) and Conf (for the probability that the chosen option is best). The variations of Val and Conf with distance, conditioned on choice consistency (i.e., on whether or not the best-rated option was chosen), are shown in Extended Data Fig. 1-1. Val globally decreased with distance (mean $r = -0.27$), irrespective of choice consistency. The distribution of choice trials reflects the variations along horizontal and vertical lines, corresponding to the blocks with constant mean and constant distance, respectively. Conf globally increased with distance (mean $r = -0.49$), but the slope depended on choice consistency: it was positive for consistent choices and negative in inconsistent choices. This pattern demonstrates a well-known property of confidence, which increases with evidence when choice is correct, and decreases when choice is incorrect (Sanders et al., 2016; Urai et al., 2017; Rouault et al., 2023). The reverse pattern was observed with RT, as could be expected from the negative relationship between Conf and RT (mean $r = -0.29$), which has been repeatedly observed (e.g., De Martino et al., 2013; Clairis & Pessiglione, 2022).

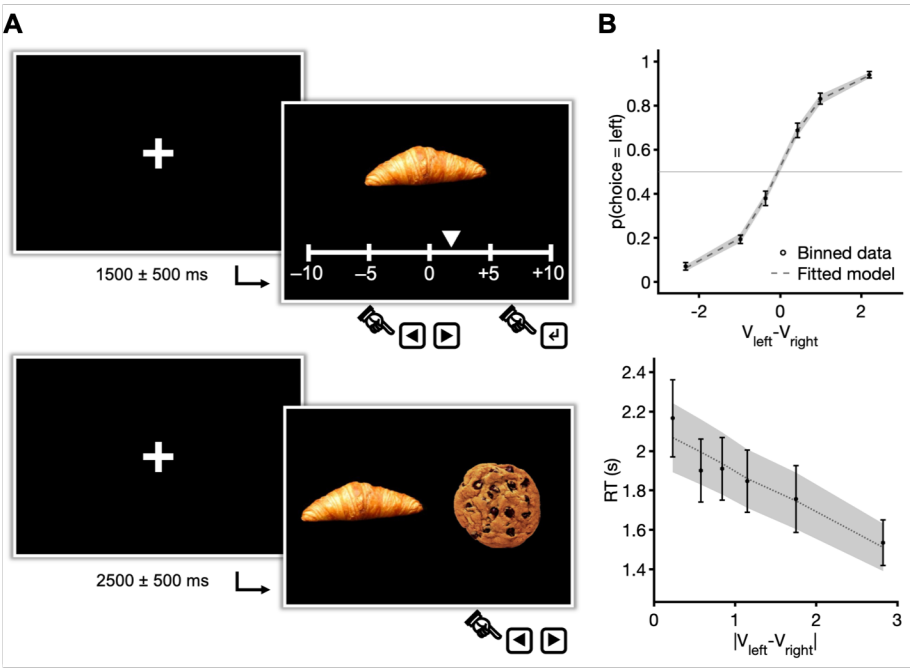

Figure 1. Behavioral tasks and results.

A) Example task trials. Successive screenshots are shown from left to right, with durations in milliseconds (except for responses, which were self-paced). *Top panels:* in the rating task (short version), participants rated the likeability of food items by moving a cursor on a visual analog scale (as reported in Lopez-Persem et al., 2020). The cursor was moved using the left and right arrows of the keyboard and the rating was validated by pressing the space bar. *Bottom panels:* in the choice task (short version), participants selected their preferred food item by pressing the left or right arrow of the keyboard.

B) Behavioral results of participants with electrodes implanted in the orbitofrontal cortex (OFC, n = 26). *Left panel:* choice rate was fitted using a logistic regression against the signed decision value (difference between left and right option values). *Right panel*: response time (RT) was fitted using a linear regression against the unsigned decision value. In both graphs, error bars and shaded areas are inter-participant SEM of observed data and model fits, respectively. See Extended Data Figure 1-1 for the distributions of value, confidence and RT plotted as a function of distance and conditioned on choice consistency.

iEEG activity

We took advantage of electrodes implanted in a total of 26 patients to record iEEG activity from 204 contacts (Fig. 2) located in the lOFC, defined as in our previous study (Lopez-Persem et al., 2020) using the Automated Anatomical Labeling (AAL, see Methods) by merging the vmPFC (n = 66 sites: 1 to 9 sites per patient, mean of 2.64 ± 0.37 sites) and lOFC (n = 138 sites: 1 to 16 sites per patient, mean of 5.75 ± 0.80 sites).

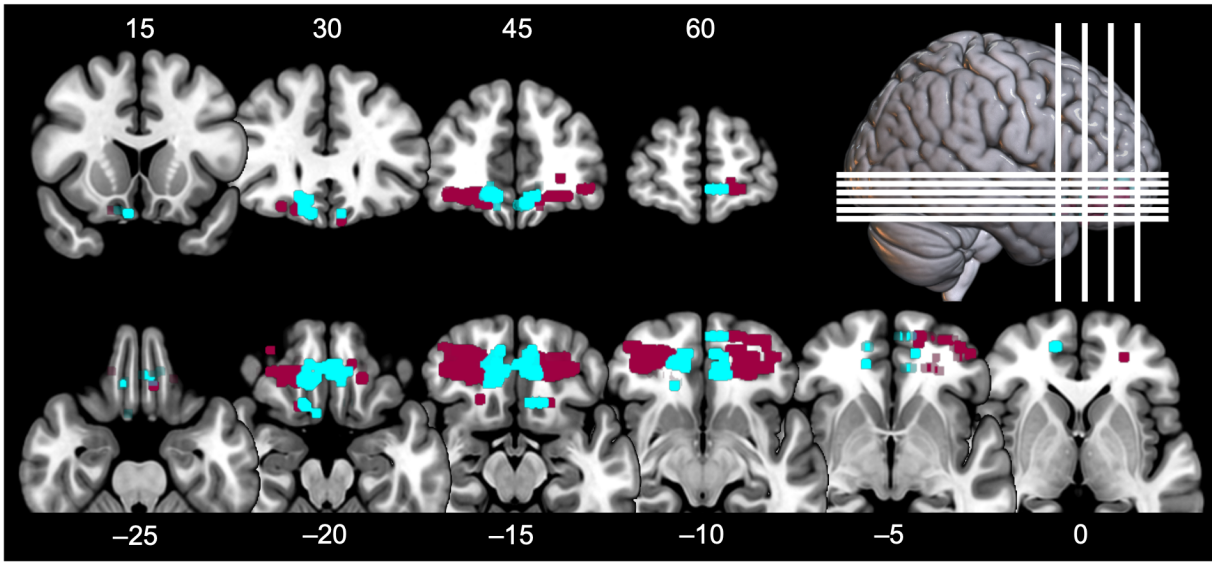

Figure 2. Anatomical localization of recording sites in the orbitofrontal cortex (OFC).

Each recording site was positioned in the MNI space and labelled according to the AAL atlas, as explained in Lopez-Persem et al. (2020). Colored voxels show the location of recording sites in the ventromedial prefrontal cortex (vmPFC, 66 sites in cyan) and the lateral orbitofrontal cortex (lOFC, 138 sites in magenta). Frontal slices at the top and axial slices at the bottom correspond to planes illustrated with vertical and horizontal bars, respectively, on the lateral view of the brain (in the top left corner). Numbers indicate their MNI y and z coordinates (in mm).

We first examined which frequency bands would show power modulation during the choice process relative to baseline. The time/frequency decomposition of trial-wise iEEG signals (full range: 2-150 Hz) revealed a significant power increase in low-frequency activity (Fig. 3A), around the θ range (4-8 Hz), that started with stimulus onset and ended with button press. There was also a significant power decrease in higher frequency bands, around the β range (13-30 Hz), that lasted after button press and was previously described as movement-related desynchronization (e.g., Meyniel & Pessiglione, 2014). When doing this analysis separately for vmPFC and lOFC recording sites (Extended Data Fig. 3-1A), we observed a qualitatively similar pattern in the two regions but a weaker θ increase in the vmPFC relative to lOFC, probably due to a lower number of electrodes implanted in this region.

To investigate the neural correlates of value and confidence, we focused on the θ range, because it showed the highest evoked response in our dataset and because the electrophysiological correlates of value sum and difference were previously observed in a low-frequency range (Hunt et al., 2012). The parametric modulation of iEEG activity across trials was investigated by fitting to every time point a

GLM that included our regressors of interest (Val and Conf) together with a trial-wise baseline (mean signal between –1 and 0 s pre-stimulus), as well as trial number and reaction time (RT). Surprisingly, regression estimates were more clearly modulated when time-locking iEEG signals to the response and showed opposite signs for Val and Conf (Fig. 3B). Indeed, θ power was negatively correlated with Val (from –0.61 to 0.25 s post-response, with peak $\beta_{Val} = -0.032 \pm 0.009$, $t_{Val}(203) = -3.65$, $p_{Val} = 3.38 \cdot 10^{-4}$) and positively correlated with Conf (from 0.016 to 0.41 s post-response, with peak $\beta_{Conf} = 0.028 \pm 0.007$, $t_{Conf}(203) = 4.01$, $p_{Conf} = 8.53 \cdot 10^{-5}$). Of note, this result remained significant when including patient identity as a random factor in the group-level analysis (within the [–0.5 s, 0.5 s] time window: $\beta_{Val} = -0.014 \pm 0.004$, $t_{Val}(203) = -3.48$, $p_{Val} = 6.22 \cdot 10^{-4}$; $\beta_{Conf} = 0.010 \pm 0.005$, $t_{Conf}(203) = 2.01$, $p_{Conf} = 4.59 \cdot 10^{-2}$), suggesting that it was not driven by a minority of individuals.

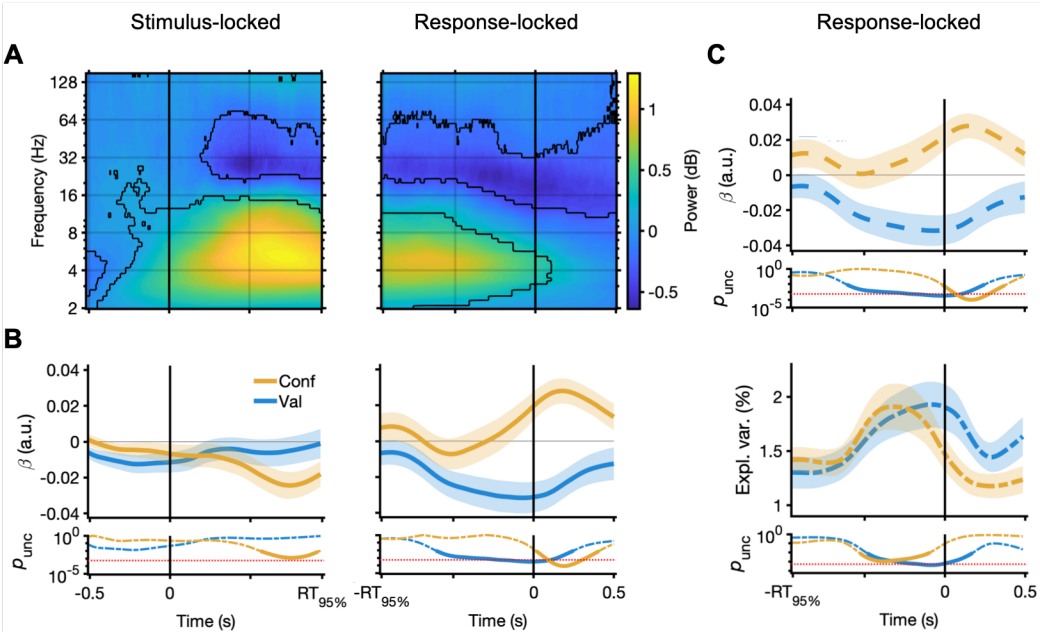

Figure 3. Val and Conf signals in low-frequency iEEG activity.

For each recording site located in the OFC, trial-by-trial iEEG time series were time-locked either to stimulus onset (*left panels*) or button press (*right panels*). The time window is restricted to the interval around choice ($RT_{95\%}$ is the duration at which choice is still ongoing in 95% of trials; $-RT_{95\%}$ is the time at which options are already on screen in 95% of trials). The same analysis was applied to each site and results were then averaged across sites.

A) Time-frequency decomposition of the evoked response. Power at each frequency is corrected for baseline activity (mean over a 1-s pre-stimulus time window). Contour lines indicate significant clusters surviving Bonferroni correction for multiple

comparisons. For the results of the same analysis considering each separate sub-region (the vmPFC and the OFC), see Extended Data Figure 3-1.

B) Time course of Val and Conf regression estimates (β). At each time point, power in the θ range (4-8 Hz) was regressed against Val and Conf, which were orthogonalized and included in the same GLM. Significance level (uncorrected p-value) is estimated using a t-test of regression estimates against zero, across recording sites. Horizontal red dotted lines indicate the Bonferroni-corrected statistical threshold; p-values are highlighted in bold when they survive correction based on random-field theory (RFT). For the results of the same analysis considering each separate sub-region (the vmPFC and the OFC), see Extended Data Figure 3-1.

C) Variants of the response-locked analysis presented in panel B, with Val and Conf regression coefficients estimated from two separate GLMs (top graph) or with explained variance instead of regression estimates (bottom graph). In the latter case, chance level under the null hypothesis was estimated using permutations (see Methods).

When doing this analysis separately for the two OFC subregions (Extended Data Fig. 3-1B), we observed that the association with Val was significant in the vmPFC and the association with Conf was significant in the lOFC sites. However, we could not conclude for a dissociation, because the effects were qualitatively similar in the two regions (just passing the threshold in one case and not the other). They both showed a stronger association (negative for Val and positive for Conf) with iEEG activity when time-locked to responses rather than stimuli.

These results confirm the presence of information about overall value and choice confidence in low-frequency OFC activity, over a peri-response time period. To check that the results were not artefacted by the orthogonalization of Val and Conf regressors when included in a single GLM, we repeated the regression analysis with a GLM that contained only Val (without Conf) or only Conf (without Val), plus the regressors of no interest. The results (Fig. 3C, top panel) were virtually unchanged, showing that Val and Conf were capturing separate parts of variance in iEEG activity. Then we conducted an analysis that is agnostic about the sign of correlation by reversing the logic and computing how much variance in value and confidence would be explained by iEEG activity (Fig. 3C, bottom panel). Significant information about Val was found from –0.48 to 0.17 s post-response (peak $r^2_{Val} = 1.92 \pm 0.21\%$, $t_{Val}(203) = 3.39$, $p_{Val} = 4.20 \cdot 10^{-4}$) and significant information about Conf from –0.53 to –0.094 s post-response (peak $r^2_{Conf} = 1.91 \pm 0.21\%$, $t_{Conf}(203) = 3.05$, $p_{Conf} = 1.30 \cdot 10^{-3}$). This

analysis confirmed the presence of both value and confidence representations in OFC low-frequency activity, peaking at about the same time just before the response.

To explore whether associations with Val and Conf would be present in other frequency bands, we extended the GLM analysis to the full time/frequency space (Fig. 4A). Although the negative correlation with Val and positive correlation with Conf are visible in the low-frequency area (4-8 Hz), no cluster survived correction for multiple comparisons, due to the high number of time/frequency data points. However, a simple median-split analysis, comparing trials with high vs. low Val and high vs. low Conf, yielded globally similar maps but with significant clusters (Fig. 4B). This analysis extends our conclusions based on θ-range activity, the negative association with Val being also observed in δ-range, α-range and β-range clusters, and the positive association with Conf in α-range clusters, all emerging within a peri-response time window (i.e., [–0.5 s, 0.5 s] around choice).

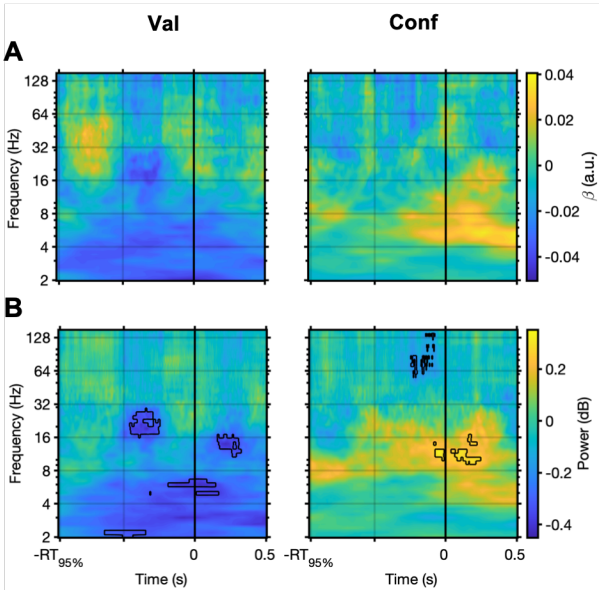

Figure 4. Val and Conf signals across frequency bands of iEEG activity.

For each recording site located in the OFC, trial-by-trial iEEG time series were time-locked to button press and epoched around choice ($-RT_{95\%}$ is the time at which options are already on screen in 95% of trials). The same analysis was applied to each site and results were then averaged across sites.

A) Regression estimates obtained for Val (*left map*) and Conf (*right map*) regression estimates.

B) Contrasted power between high vs. low Val (*left map*) or high vs. low Conf (*right map*). High and low trials were identified using a median split. Contour lines indicate significant clusters surviving Bonferroni correction for multiple comparisons.

Then we examined the spatial distribution of Val and Conf signals, meaning Val and Conf regression weights in explaining θ activity, extracted from the [–0.5 s, 0.5 s] time window. There was no particular pattern for Val and Conf signals distribution (Fig. 5A) along the mediolateral axis, which distinguishes vmPFC and lOFC regions. Among the 204 recording sites, 16 showed a significant correlation with Val only, 17 with Conf only, and 3 with both (Fig. 5B). This is not different from what could be expected if the two signals were independent from each other ($\chi^2 = 1.01$, $p = 0.32$). Although correlation was negative with Val and positive with Conf over the entire set of recordings, small clusters of recording sites showed significant opposite signals (positive with Val or negative with Conf). However, these clusters also failed to show significant correlations of the same sign with both Val and Conf (i.e., both Val-positive and Val-negative clusters failed to signal Conf, and both Conf-positive and Conf-negative clusters failed to signal Val). Recording sites with regression weights of the same sign for Val and Conf should cluster in the bottom left and top right quadrants of the 2D distribution, which was not observed (Fig. 5B). Overall, there was no correlation between Val and Conf signals across recording sites ($r = 0.06$, $p = 0.42$).

To test for the presence of a Val-to-Conf gradient from posteroventral to anterodorsal regions (De Martino et al., 2017; Clairis & Pessiglione, 2022), we regressed the difference between Val and Conf signals against MNI coordinates projected along the yz-axis (Fig. 5C). This gradient was indeed significant ($\beta_{yz} = 4.11 \cdot 10^{-3} \pm 1.70 \cdot 10^{-3}$, $t_{yz}(202) = 2.42$, $p_{yz} = 1.66 \cdot 10^{-2}$). However, a systematic regression of Val and Conf signals against each of the 3 axes separately (Extended Data Fig. 5-1) showed that the gradient was driven by Conf representation being more dorsal – this being the only association that survived Bonferroni correction for multiple tests ($\beta_z = 6.30 \cdot 10^{-3}$, $t_z(202) = 3.03$, $p_z = 2.80 \cdot 10^{-3}$).

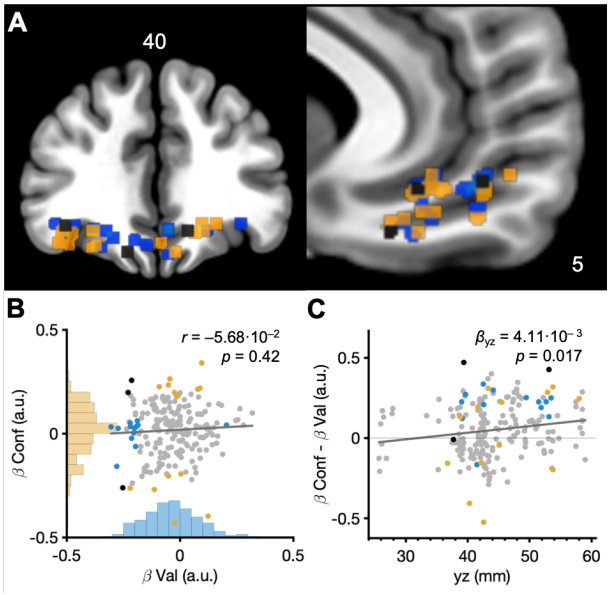

Figure 5. Distribution of Val and Conf signals across recording sites.

A) Localization of Val and Conf signals. Significant recording sites (blue for Val, orange for Conf, black for both) are superimposed on frontal and sagittal slices of the anatomical MNI brain template (taken at y = 40 mm and x = 5 mm, respectively). Significance was assessed using a GLM fitted to the mean signal in the θ range (4-8 Hz), extracted from the [–0.5 s, 0.5 s] time window surrounding choice (button press).

B) Correlation between Val and Conf β regression estimates across recording sites. Dots are recording sites and *r* is Pearson's correlation coefficient. The dark grey line shows the linear regression fit and bars the marginal distributions of β regression estimates.

C) Gradient of Val and Conf signals along a posteroventral to anterodorsal (yz) axis. Dots are recording sites and β_{yz} is the estimate from the regression of the difference between Conf and Val β estimates against the coordinates projected onto the yz-axis. For the gradient of Val and Conf along each separate axis (x, y, z), see Extended Data Figure 5-1.

To further specify Val and Conf signals, we analyzed separately the pool of recording sites that were driving the main global results: significant negative association with Val ("Val–" sites, n = 15) or significantly positive correlation with Conf ("Conf+" sites, n = 10). When using our main GLM, the dissociation was confirmed (Fig. 6A, top panels): Val– sites were insensitive to confidence and Conf+ sites were insensitive to value. When replacing Val and Conf in the GLM by the values of chosen and unchosen options (V_{Ch} and V_{Unch}), regression estimates (Fig. 6A, middle panels) confirmed that Val– sites were signaling the two options with the same sign (for V_{Ch}: peak $\beta_{Ch} = -0.18 \pm 0.031$, $t_{Ch}(14) = -5.72$, $p_{Ch} = 5.29 \cdot 10^{-5}$; for V_{Unch}: peak $\beta_{Unch} = -0.15 \pm 0.024$, $t_{Unch}(14) = -6.19$, $p_{Unch} = 2.36 \cdot 10^{-5}$), whereas

Conf+ sites were signaling the two options with opposite signs (for V_{Ch}: $\beta_{Ch} = 0.12 \pm 0.022$, $t_{Ch}(9) = 5.57$, $p_{Ch} = 3.48 \cdot 10^{-4}$; for V_{Unch}: peak $\beta_{Unch} = -0.13 \pm 0.027$, $t_{Unch}(9) = -4.65$, $p_{Unch} = 1.20 \cdot 10^{-3}$).

When replacing Val and Conf by RT in the GLM (Fig. 6A, bottom panels), we observed no significant correlate in Val– sites, but a significant negative association in Conf+ sites (peak $\beta_{RT} = -0.18 \pm 0.061$, $t_{RT}(9) = -3.00$, $p_{RT} = 1.49 \cdot 10^{-2}$). This strengthens the interpretation that Conf+ sites reflect confidence, given that confidence is lower when RT is longer. As shown in Extended Data Fig. 1-1, confidence-signaling activity is expected to increase with both choice easiness (distance between option values) and choice consistency (selection of best-rated option). We tested these predictions on θ activity recorded in Val– sites and Conf+ sites (Fig. 6B): we found no effect in Val– sites, but θ activity in Conf+ sites was higher when choices were easier ($t_{easiness}(11) = 4.30$, $p_{easiness} = 1.27 \cdot 10^{-3}$) and consistent ($t_{consistency}(11) = 6.30$, $p_{consistency} = 5.82 \cdot 10^{-5}$), following the expected signature of a confidence signal.

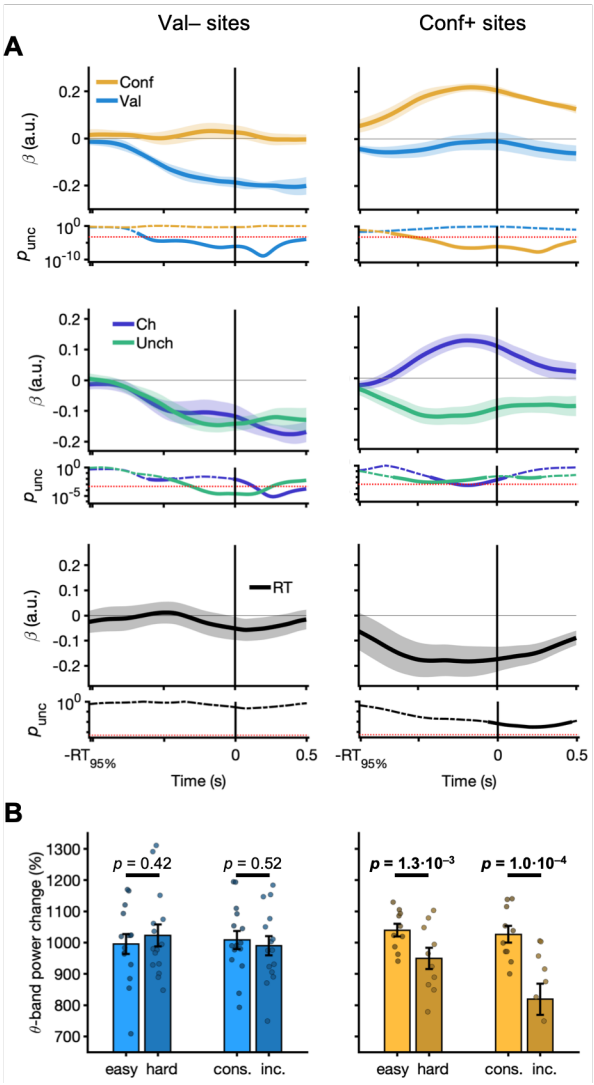

Figure 6. Decomposition of Val and Conf signals.

Left and right columns show results pooled over recording sites driving Val and Conf signals, meaning sites for which θ-range (4-8 Hz) activity extracted from the [–0.5 s, 0.5 s] time window surrounding choice (button press) is negatively associated with Val and positively associated with Conf (blue and orange sites in Fig. 4).

A) Time course of Val and Conf β regression estimates. At each time point, power in the θ range (4-8 Hz) was regressed against a GLM including as regressors either Val and Conf (same as in Fig. 3; top panels), chosen and unchosen option values (not orthogonalized; middle panels), or response time (RT; bottom panels). Significance level (uncorrected p-value) is estimated using a t-test of regression estimates against zero, across recording sites. Horizontal red dotted lines indicate the Bonferroni-corrected statistical threshold; p-values are highlighted in bold when they survive correction based on random-field theory (RFT).

B) Effects of choice consistency and choice easiness. θ-range (4-8 Hz) activity extracted from the [–0.5 s, 0.5 s] time window surrounding choice (button press) was averaged separately for consistent and inconsistent trials (when the best-rated option was chosen and not chosen) and for easy and hard trials (sorted by a median split on the distance between option values). Dots

are recording sites, bars and error bars are means and standard errors of the mean. Bold p-values indicate the differences that survived Bonferroni correction.

Model simulation

Finally, we examined whether the value and confidence signals observed here could arise from a comparison process, as was previously argued by Hunt and colleagues in their seminal paper (2012). Indeed, low-frequency MEG activity reconstructed from a vmPFC region was found to signal the sum and difference of option values in a binary choice task, which was interpreted as reflecting the activity of neural network implementing the comparison between options. This comparison mechanism can be simulated in an artificial neural network (ANN; Wang, 2002; Wong et al., 2007), where two distinct excitatory units take as input the values of the two options, and compete with each other through reciprocal inhibition (Fig. 7A). When the two options are made available, a competition emerges until one pyramidal unit overruns and silences the other, while reaching a plateau that triggers the selection of the associated option. We adapted the ANN used by Hunt and colleagues to reproduce the mean rate of consistent choices and the mean RT of our patients, using their likeability ratings. Simulated activity of the ANN was then analyzed with the same GLM as was done with observed OFC iEEG activity. Results replicate the pattern reported by Hunt and colleagues and extend to Val and Conf signals (Fig. 7B), which was expected given that Val is nothing but the sum of option values, and Conf a sigmoid transformation of the difference between chosen and unchosen option values.

However, there were key differences between simulated and real data. First, Val and Conf signals only appear when time-locked to the response in OFC data, whereas time-locking does not matter in simulated data. Second, Val and Conf signals have opposite signs in OFC data, whereas there are both positive in simulated data. Third, different recording sites in the OFC only pick up either Val or Conf signal, whereas an electrode at the vicinity of the ANN would necessarily pick up both Val and Conf signals.

Thus, low-frequency iEEG activity in the OFC was more compatible with sparse coding of value and confidence estimates that build up in the course of choice deliberation, rather than reflecting a single mechanism comparing ready-made option values.

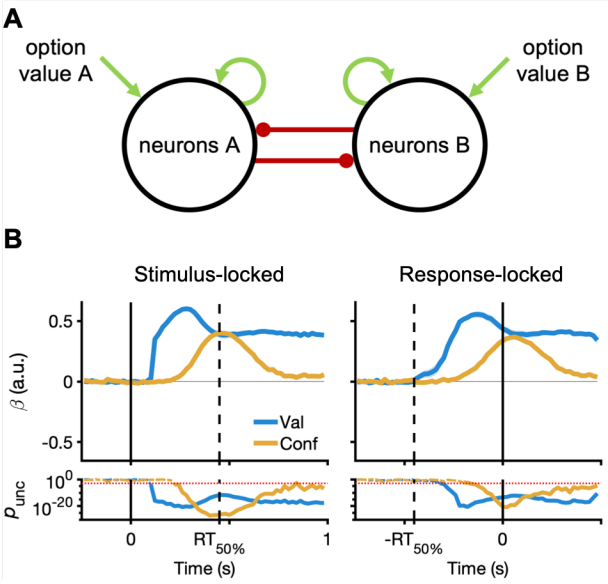

Figure 7. Simulations of the attractor network model.

A) The model (borrowed from Hunt et al., 2012) simulates a competition, via mutual inhibition, between two self-excitatory units, each taking as input one of the two option values. The model has been adapted to the choices made by each of the 26 participants, using likeability ratings as option values. A decision is made when the difference in activity between the two units reaches a plateau. The input is stopped 1 s after the onset of choice options, to roughly match the average $RT_{95\%}$ (time at which the choice is still ongoing in 95% of trials) observed in our participants.

B) At each time point, the total activity of this simple network has been regressed against Val and Conf, meaning the overall value (Ch + Unch) and the choice probability, which is a sigmoid transform of the value difference (Ch – Unch). The left and right panels show the time course of regression estimates (top) and significance levels (bottom) when activity is locked to stimulus onset and to button press, respectively. Significance level (uncorrected p-value) is estimated using a t-test of regression estimates against zero, across the 26 simulated participants. Horizontal red dotted lines indicate the Bonferroni-corrected statistical threshold; p-values are highlighted in bold when they survive correction based on random-field theory (RFT). Vertical black dotted lines indicate median RT across trials ($RT_{50\%}$).

Discussion

In this study, we took advantage of electrodes implanted in the OFC of patients with pharmaco-resistant epilepsy to investigate value and confidence signals during preference-based decisions. We observed that low-frequency OFC activity reflected both constructs Val (sum of option values) and Conf (probability that chosen option is best).

The correlation with Val is consistent with the general idea that the OFC is part of the brain valuation system (Schultz, 2006; Padoa-Schioppa, 2007; Rangel et al., 2008; Bartra et al., 2013), whose signals may provide a common neural currency for ordering choice options (Montague & Berns, 2002; D. J. Levy & Glimcher, 2012). However, this correlation does not tell whether OFC activity signals the overall value of the option set, as previously suggested (Shenhav & Karmarkar, 2019), or represents separate estimates for the two option values, which would be aggregated in the recorded signal. When introduced as separate regressors in the general linear model, option values were both reflected in the activity of Val-signaling sites, with similar temporal dynamics. This pattern seems to suggest that the two value estimates are generated simultaneously, but it could also come from averaging even if options are valuated alternatively. Indeed, if the sequence of option exploration differs between participants or between trials, the temporal alignment of option value signals would be blurred. The issue might be solved by monitoring eye movements, if we assume that the OFC signals the value of the option that is looked at, as suggested in some versions of sequential sampling models (e.g., Krajbich et al., 2010). The value signal observed here is indeed compatible with a neural network model that transforms a set of attributes into a distribution of activity that can be decoded by downstream neurons to infer the value of attended and unattended options (Pessiglione & Daunizeau, 2021). To further test this model, it would be necessary to know which option is attended at any time point and to simultaneously record a distribution of neural activities. With the present dataset, multivariate decoding was not feasible because recording sites were sampled in different patients making different choices.

The correlation with Conf is consistent with a wealth of studies that reported representation of confidence in OFC activity, not only during preference-based decision or judgment (De Martino et al., 2013; Lebreton et al., 2015; Bobadilla-Suarez et al., 2020; Lopez-Persem et al., 2020; Shapiro & Grafton, 2020), but also perception-based or memory-based decisions (Chua et al., 2006; Bang &

Fleming, 2018; Gherman & Philiastides, 2018; Morales et al., 2018; Rouault et al., 2023). Further investigation showed that the pattern of low-frequency activity recorded by Conf sites was consistent with a notion of confidence: it increased with chosen option value and decreased with unchosen option value, it was higher both when choice was easier (more distance between option values) and when choice was right (the best-rated option being selected), and it was also associated with shorter choice RT. Yet, one limitation of these results is that we use a proxy for confidence and not the confidence reported by the participant. Previous studies nevertheless showed that our confidence proxy is tightly correlated to confidence rating (Clairis & Pessiglione, 2022) and that both were correlated with iEEG activity in the OFC (Lopez-Persem et al., 2020).

It could be argued that the inclusion of Val and Conf regressors in the same GLM might induce spurious correlations since they share one variable (chosen option value). This was not the case however, because the same result was obtained whether the two regressors were orthogonalized and tested in a same GLM or tested in separate GLMs. Regarding the dynamics, Val signals were observed slightly before Conf signals in the parametric regression analysis (with Val just before and Conf just after the response), but not in the explained variance analysis (in which the two signals peaked before the response). We note that results are also mixed in fMRI studies (which may have insufficient time resolution), some claiming that values are signaled before confidence (e.g., Shapiro & Grafton, 2020) and others that the two variables are simultaneously represented in vmPFC activity (e.g., Lebreton et al., 2015). The anteriority of value over confidence makes sense in the view that values are provided for the comparison and selection to take place, but not in the view that option values are constructed on the fly, simultaneously to the decision-making process. A recent account of decision-making (Lee & Daunizeau, 2021) suggested that option values are refined until the tradeoff between the expected confidence gain and the required deliberation time becomes disadvantageous. For the implementation of such tradeoff mechanism, option values and choice confidence would need to be simultaneously represented.

Regarding the frequency range, the negative correlation between option value and low-frequency activity was already reported in iEEG studies during rating or bidding tasks where options were presented one at a time (Lopez-Persem et al., 2020; Shih et al., 2023). When extending the analysis

to the full frequency spectrum, we observed that the negative/positive correlation with value/confidence was globally true, with significant clusters in higher frequency ranges (classically labeled α and β). The absence of significant correlate in high frequencies may be surprising, as most iEEG studies reported equivalents of BOLD responses in broadband gamma activation (Jerbi et al., 2009; Lachaux et al., 2012), including recent studies using similar recording and analytic methods, but a task requiring just one value estimate per trial (Lopez-Persem et al., 2020; Cecchi et al., 2022; Shih et al., 2023). One explanation could be that value and confidence signals follow gaze fixation (i.e., which option is considered for selection) and therefore would only appear in low-frequency activity because temporal smoothing would compensate for misalignment of visual saccades.

Regarding the spatial distribution, OFC signals appeared to shift from value to confidence along the posterior-to-anterior and ventral-to-dorsal axis. This replicates, within the OFC, the value-to-confidence gradient that was previously documented along the medial prefrontal cortex (De Martino et al., 2017; Clairis & Pessiglione, 2022). This gradient might reflect some overlapping, but independent, distributed codes for value and confidence across OFC subregions. It should be noted that, as in our previous iEEG study (Lopez-Persem et al., 2020), there was no clear dissociation between vmPFC and lOFC subregions, both containing recording sites with significant value and confidence signals. This is at odds with fMRI studies, which typically find correlates of value and confidence in ventromedial but not ventrolateral prefrontal regions (Bartra et al., 2013; Clithero & Rangel, 2014; Vaccaro & Fleming, 2018). However, electrophysiological recordings in monkeys also identified value signals in lateral parts of the OFC (Rich & Wallis, 2016; Hunt et al., 2018; Pastor-Bernier et al., 2021). Thus, iEEG recordings in patients may offer a bridge between human fMRI and monkey electrophysiology results. It remains unclear why fMRI studies generally fail to demonstrate correlates of value in the lOFC. This might come from a lack of sensitivity due to the proximity of air-filled sinuses, or to a more stringent correction for multiple comparisons in whole-brain analyses given the large number of voxels, or to a higher individual variability in the location of value-signaling voxels that would weaken group-level statistics.

Finally, we compared the value and confidence signals observed in OFC activity with those generated by an attractor network model implementing a comparison between option values (Hunt et al., 2012). While both expressed value and confidence signals, real OFC activity differed from simulated

activity on several key points. First, value and confidence signals only appeared when time-locking OFC activity to response onset (not stimulus onset), suggesting that these representations were not input to the system but constructions that triggered the decision when fully achieved. Second, the sign of correlation with OFC activity was opposite for value and confidence, contradicting the predictions of the comparison mechanism. Third, value and confidence signals were recorded in distinct locations, violating the assumption that they could arise from a same attractor neural network. Overall, the pattern of OFC activity observed here was more compatible with the idea of a large neural population transforming the attributes of choice options into sparsely coded value and confidence estimates that may be readout by different downstream neurons (Pessiglione & Daunizeau, 2021).

Although patients tested here suffered from epilepsy, we treated iEEG activity recorded in their OFC as stemming from a normal brain. This is reasonable given that epileptic foci were located outside the OFC, that epileptic artifacts were removed from raw recordings, and that epileptic events were unlikely to coincide with value and confidence constructs anyway. Yet our findings may provide insight into the consequences of OFC damage for decision-making. Rather than being unable to compare values, patients with partial OFC lesions may have distorted value and confidence signals, depending on which neurons are impaired with respect to the readout codes. If confidence is indeed driving the meta-cognitive control of decisions, lesioned patients may be unable to adjust the deliberation process, hence making poor decisions with high confidence or vice-versa.

643 **References**

644 Abitbol, R., Lebreton, M., Hollard, G., Richmond, B. J., Bouret, S., & Pessiglione, M. (2015). Neural
645 Mechanisms Underlying Contextual Dependency of Subjective Values: Converging Evidence
646 from Monkeys and Humans. *Journal of Neuroscience*, *35*(5), 2308–2320.
647 https://doi.org/10.1523/JNEUROSCI.1878-14.2015

648 Bang, D., & Fleming, S. M. (2018). Distinct encoding of decision confidence in human medial
649 prefrontal cortex. *Proceedings of the National Academy of Sciences*, *115*(23), 6082–6087.
650 https://doi.org/10.1073/pnas.1800795115

651 Bartra, O., McGuire, J. T., & Kable, J. W. (2013). The valuation system: A coordinate-based meta-
652 analysis of BOLD fMRI experiments examining neural correlates of subjective value.
653 *NeuroImage*, *76*, 412–427. https://doi.org/10.1016/j.neuroimage.2013.02.063

654 Bénon, J., Lee, D., Hopper, W., Verdeil, M., Pessiglione, M., Vinckier, F., Bouret, S., Rouault, M.,
655 Lebouc, R., Pezzulo, G., Schreiweis, C., Burguière, E., & Daunizeau, J. (2024). The online
656 metacognitive control of decisions. *Communications Psychology*, *2*(1), 1–17.
657 https://doi.org/10.1038/s44271-024-00071-y

658 Bobadilla-Suarez, S., Guest, O., & Love, B. C. (2020). Subjective value and decision entropy are
659 jointly encoded by aligned gradients across the human brain. *Communications Biology*, *3*(1),
660 Article 1. https://doi.org/10.1038/s42003-020-01315-3

661 Cecchi, R., Vinckier, F., Hammer, J., Marusic, P., Nica, A., Rheims, S., Trebuchon, A., Barbeau, E. J.,
662 Denuelle, M., Maillard, L., Minotti, L., Kahane, P., Pessiglione, M., & Bastin, J. (2022).
663 Intracerebral mechanisms explaining the impact of incidental feedback on mood state and
664 risky choice. *eLife*, *11*, e72440. https://doi.org/10.7554/eLife.72440

665 Chau, B. K. H., Kolling, N., Hunt, L. T., Walton, M. E., & Rushworth, M. F. S. (2014). A neural
666 mechanism underlying failure of optimal choice with multiple alternatives. *Nature*
667 *Neuroscience*, *17*(3), 463–470. https://doi.org/10.1038/nn.3649

668 Chua, E. F., Schacter, D. L., Rand-Giovannetti, E., & Sperling, R. A. (2006). Understanding
669 metamemory: Neural correlates of the cognitive process and subjective level of confidence in

recognition memory. *NeuroImage*, *29*(4), 1150–1160. https://doi.org/10.1016/j.neuroimage.2005.09.058

Clairis, N., & Pessiglione, M. (2022). Value, Confidence, Deliberation: A Functional Partition of the Medial Prefrontal Cortex Demonstrated across Rating and Choice Tasks. *The Journal of Neuroscience*, *42*(28), 5580–5592. https://doi.org/10.1523/JNEUROSCI.1795-21.2022

Clithero, J. A., & Rangel, A. (2014). Informatic parcellation of the network involved in the computation of subjective value. *Social Cognitive and Affective Neuroscience*, *9*(9), 1289–1302. https://doi.org/10.1093/scan/nst106

Daunizeau, J., Adam, V., & Rigoux, L. (2014). VBA: A Probabilistic Treatment of Nonlinear Models for Neurobiological and Behavioural Data. *PLOS Computational Biology*, *10*(1), e1003441. https://doi.org/10.1371/journal.pcbi.1003441

De Martino, B., Bobadilla-Suarez, S., Nouguchi, T., Sharot, T., & Love, B. C. (2017). Social Information Is Integrated into Value and Confidence Judgments According to Its Reliability. *The Journal of Neuroscience*, *37*(25), 6066–6074. https://doi.org/10.1523/JNEUROSCI.3880-16.2017

De Martino, B., Fleming, S. M., Garrett, N., & Dolan, R. J. (2013). Confidence in value-based choice. *Nature Neuroscience*, *16*(1), 105–110. https://doi.org/10.1038/nn.3279

García-Pérez, E., Mahfooz, K., Covita, J., Zandueta, A., & Wesseling, J. F. (2015). Levetiracetam accelerates the onset of supply rate depression in synaptic vesicle trafficking. *Epilepsia*, *56*(4), 535–545. https://doi.org/10.1111/epi.12930

Gherman, S., & Philiastides, M. G. (2018). Human VMPFC encodes early signatures of confidence in perceptual decisions. *eLife*, *7*, e38293. https://doi.org/10.7554/eLife.38293

Gläscher, J., Hampton, A. N., & O'Doherty, J. P. (2009). Determining a Role for Ventromedial Prefrontal Cortex in Encoding Action-Based Value Signals During Reward-Related Decision Making. *Cerebral Cortex*, *19*(2), 483–495. https://doi.org/10.1093/cercor/bhn098

Glimcher, P. W., & Rustichini, A. (2004). Neuroeconomics: The Consilience of Brain and Decision. *Science*, *306*(5695), 447–452. https://doi.org/10.1126/science.1102566

Hunt, L. T., Kolling, N., Soltani, A., Woolrich, M. W., Rushworth, M. F. S., & Behrens, T. E. J. (2012). Mechanisms underlying cortical activity during value-guided choice. *Nature Neuroscience*, *15*(3), 470–476. https://doi.org/10.1038/nn.3017

Hunt, L. T., Malalasekera, W. M. N., de Berker, A. O., Miranda, B., Farmer, S. F., Behrens, T. E. J., & Kennerley, S. W. (2018). Triple dissociation of attention and decision computations across prefrontal cortex. *Nature Neuroscience*, *21*(10), 1471–1481. https://doi.org/10.1038/s41593-018-0239-5

Jenkinson, M., Beckmann, C. F., Behrens, T. E. J., Woolrich, M. W., & Smith, S. M. (2012). FSL. *NeuroImage*, *62*(2), 782–790. https://doi.org/10.1016/j.neuroimage.2011.09.015

Jerbi, K., Ossandón, T., Hamamé, C. M., Senova, S., Dalal, S. S., Jung, J., Minotti, L., Bertrand, O., Berthoz, A., Kahane, P., & Lachaux, J.-P. (2009). Task-related gamma-band dynamics from an intracerebral perspective: Review and implications for surface EEG and MEG. *Human Brain Mapping*, *30*(6), 1758–1771. https://doi.org/10.1002/hbm.20750

Krajbich, I., Armel, C., & Rangel, A. (2010). Visual fixations and the computation and comparison of value in simple choice. *Nature Neuroscience*, *13*(10), Article 10. https://doi.org/10.1038/nn.2635

Lachaux, J.-P., Axmacher, N., Mormann, F., Halgren, E., & Crone, N. E. (2012). High-frequency neural activity and human cognition: Past, present and possible future of intracranial EEG research. *Progress in Neurobiology*, *98*(3), 279–301. https://doi.org/10.1016/j.pneurobio.2012.06.008

Lachaux, J.-P., Rudrauf, D., & Kahane, P. (2003). Intracranial EEG and human brain mapping. *Journal of Physiology-Paris*, *97*(4–6), 613–628. https://doi.org/10.1016/j.jphysparis.2004.01.018

Lebreton, M., Abitbol, R., Daunizeau, J., & Pessiglione, M. (2015). Automatic integration of confidence in the brain valuation signal. *Nature Neuroscience*, *18*(8), 1159–1167. https://doi.org/10.1038/nn.4064

Lebreton, M., Jorge, S., Michel, V., Thirion, B., & Pessiglione, M. (2009). An Automatic Valuation System in the Human Brain: Evidence from Functional Neuroimaging. *Neuron*, *64*(3), 431–439. https://doi.org/10.1016/j.neuron.2009.09.040

Lee, D. G., & Daunizeau, J. (2021). Trading mental effort for confidence in the metacognitive control of value-based decision-making. *eLife*, *10*, e63282. https://doi.org/10.7554/eLife.63282

Levy, D. J., & Glimcher, P. W. (2012). The root of all value: A neural common currency for choice. *Current Opinion in Neurobiology*, *22*(6), 1027–1038. https://doi.org/10.1016/j.conb.2012.06.001

Levy, I., Lazzaro, S. C., Rutledge, R. B., & Glimcher, P. W. (2011). Choice from Non-Choice: Predicting Consumer Preferences from Blood Oxygenation Level-Dependent Signals Obtained during Passive Viewing. *Journal of Neuroscience*, *31*(1), 118–125. https://doi.org/10.1523/JNEUROSCI.3214-10.2011

Lopez-Persem, A., Bastin, J., Petton, M., Abitbol, R., Lehongre, K., Adam, C., Navarro, V., Rheims, S., Kahane, P., Domenech, P., & Pessiglione, M. (2020). Four core properties of the human brain valuation system demonstrated in intracranial signals. *Nature Neuroscience*, *23*(5), 664–675. https://doi.org/10.1038/s41593-020-0615-9

Meyniel, F., & Pessiglione, M. (2014). Better Get Back to Work: A Role for Motor Beta Desynchronization in Incentive Motivation. *Journal of Neuroscience*, *34*(1), 1–9. https://doi.org/10.1523/JNEUROSCI.1711-13.2014

Montague, P. R., & Berns, G. S. (2002). Neural Economics and the Biological Substrates of Valuation. *Neuron*, *36*(2), 265–284. https://doi.org/10.1016/S0896-6273(02)00974-1

Morales, J., Lau, H., & Fleming, S. M. (2018). Domain-General and Domain-Specific Patterns of Activity Supporting Metacognition in Human Prefrontal Cortex. *Journal of Neuroscience*, *38*(14), 3534–3546. https://doi.org/10.1523/JNEUROSCI.2360-17.2018

Oostenveld, R., Fries, P., Maris, E., & Schoffelen, J.-M. (2011). FieldTrip: Open Source Software for Advanced Analysis of MEG, EEG, and Invasive Electrophysiological Data. *Computational Intelligence and Neuroscience*, *2011*, 156869. https://doi.org/10.1155/2011/156869

Padoa-Schioppa, C. (2007). Orbitofrontal Cortex and the Computation of Economic Value. *Annals of the New York Academy of Sciences*, *1121*(1), 232–253. https://doi.org/10.1196/annals.1401.011

Padoa-Schioppa, C. (2011). Neurobiology of Economic Choice: A Good-Based Model. *Annual Review of Neuroscience*, *34*(Volume 34, 2011), 333–359. https://doi.org/10.1146/annurev-neuro-061010-113648

Padoa-Schioppa, C., & Assad, J. A. (2006). Neurons in the orbitofrontal cortex encode economic value. *Nature*, *441*(7090), Article 7090. https://doi.org/10.1038/nature04676

Pastor-Bernier, A., Stasiak, A., & Schultz, W. (2021). Reward-specific satiety affects subjective value signals in orbitofrontal cortex during multicomponent economic choice. *Proceedings of the National Academy of Sciences*, *118*(30), e2022650118. https://doi.org/10.1073/pnas.2022650118

Pessiglione, M., & Daunizeau, J. (2021). Bridging across functional models: The OFC as a value-making neural network. *Behavioral Neuroscience*, *135*(2), 277–290. https://doi.org/10.1037/bne0000464

Philiastides, M. G., Biele, G., & Heekeren, H. R. (2010). A mechanistic account of value computation in the human brain. *Proceedings of the National Academy of Sciences*, *107*(20), 9430–9435. https://doi.org/10.1073/pnas.1001732107

Rangel, A., Camerer, C., & Montague, P. R. (2008). A framework for studying the neurobiology of value-based decision making. *Nature Reviews Neuroscience*, *9*(7), Article 7. https://doi.org/10.1038/nrn2357

Rich, E. L., & Wallis, J. D. (2016). Decoding subjective decisions from orbitofrontal cortex. *Nature Neuroscience*, *19*(7), 973–980. https://doi.org/10.1038/nn.4320

Rouault, M., Lebreton, M., & Pessiglione, M. (2023). A shared brain system forming confidence judgment across cognitive domains. *Cerebral Cortex*, *33*(4), 1426–1439. https://doi.org/10.1093/cercor/bhac146

Saez, I., Lin, J., Stolk, A., Chang, E., Parvizi, J., Schalk, G., Knight, R. T., & Hsu, M. (2018). Encoding of Multiple Reward-Related Computations in Transient and Sustained High-

Frequency Activity in Human OFC. *Current Biology*, *28*(18), 2889-2899.e3. https://doi.org/10.1016/j.cub.2018.07.045

Sanders, J. I., Hangya, B., & Kepecs, A. (2016). Signatures of a Statistical Computation in the Human Sense of Confidence. *Neuron*, *90*(3), 499–506. https://doi.org/10.1016/j.neuron.2016.03.025

Schultz, W. (2006). Behavioral Theories and the Neurophysiology of Reward. *Annual Review of Psychology*, *57*(1), 87–115. https://doi.org/10.1146/annurev.psych.56.091103.070229

Shapiro, A. D., & Grafton, S. T. (2020). Subjective value then confidence in human ventromedial prefrontal cortex. *PLOS ONE*, *15*(2), e0225617. https://doi.org/10.1371/journal.pone.0225617

Shenhav, A., & Karmarkar, U. R. (2019). Dissociable components of the reward circuit are involved in appraisal versus choice. *Scientific Reports*, *9*(1), Article 1. https://doi.org/10.1038/s41598-019-38927-7

Shih, W.-Y., Yu, H.-Y., Lee, C.-C., Chou, C.-C., Chen, C., Glimcher, P. W., & Wu, S.-W. (2023). Electrophysiological population dynamics reveal context dependencies during decision making in human frontal cortex. *Nature Communications*, *14*(1), Article 1. https://doi.org/10.1038/s41467-023-42092-x

Strait, C. E., Blanchard, T. C., & Hayden, B. Y. (2014). Reward Value Comparison via Mutual Inhibition in Ventromedial Prefrontal Cortex. *Neuron*, *82*(6), 1357–1366. https://doi.org/10.1016/j.neuron.2014.04.032

Suzuki, S., Cross, L., & O'Doherty, J. P. (2017). Elucidating the underlying components of food valuation in the human orbitofrontal cortex. *Nature Neuroscience*, *20*(12), Article 12. https://doi.org/10.1038/s41593-017-0008-x

Talairach, J., & Tournoux, P. (1988). *Co-Planar Stereotaxic Atlas of the Human Brain. 3-Dimensional Proportional System: An Approach to Cerebral Imaging*. Thieme Medical Publishers.

Tremblay, L., & Schultz, W. (1999). Relative reward preference in primate orbitofrontal cortex. *Nature*, *398*(6729), 704–708. https://doi.org/10.1038/19525

Tzourio-Mazoyer, N., Landeau, B., Papathanassiou, D., Crivello, F., Etard, O., Delcroix, N., Mazoyer, B., & Joliot, M. (2002). Automated Anatomical Labeling of Activations in SPM Using a

Macroscopic Anatomical Parcellation of the MNI MRI Single-Subject Brain. *NeuroImage*, *15*(1), 273–289. https://doi.org/10.1006/nimg.2001.0978

Urai, A. E., Braun, A., & Donner, T. H. (2017). Pupil-linked arousal is driven by decision uncertainty and alters serial choice bias. *Nature Communications*, *8*(1), 14637. https://doi.org/10.1038/ncomms14637

Vaccaro, A. G., & Fleming, S. M. (2018). Thinking about thinking: A coordinate-based meta-analysis of neuroimaging studies of metacognitive judgements. *Brain and Neuroscience Advances*, *2*, 2398212818810591. https://doi.org/10.1177/2398212818810591

Wang, X.-J. (2002). Probabilistic Decision Making by Slow Reverberation in Cortical Circuits. *Neuron*, *36*(5), 955–968. https://doi.org/10.1016/S0896-6273(02)01092-9

Wong, K.-F., Huk, A., Shadlen, M., & Wang, X.-J. (2007). Neural circuit dynamics underlying accumulation of time-varying evidence during perceptual decision making. *Frontiers in Computational Neuroscience*, *1*. https://www.frontiersin.org/articles/10.3389/neuro.10.006.2007

Wong, K.-F., & Wang, X.-J. (2006). A Recurrent Network Mechanism of Time Integration in Perceptual Decisions. *Journal of Neuroscience*, *26*(4), 1314–1328. https://doi.org/10.1523/JNEUROSCI.3733-05.2006

Extended Data

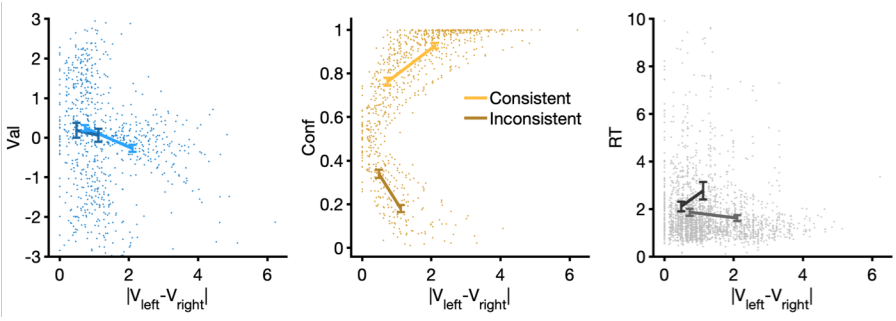

Figure 1-1. Distributions of value, confidence and RT conditioned on choice consistency.

Val, Conf and RT are plotted as a function of distance (unsigned difference between option values), with light and dark colors for consistent versus inconsistent choices (i.e., for when the best-rated option was chosen versus not chosen). Each dot is a choice trial. Lines show group-level means within two bins obtained by median-splitting the distance, separately for consistent and inconsistent trials. Error bars are standard error of the mean.

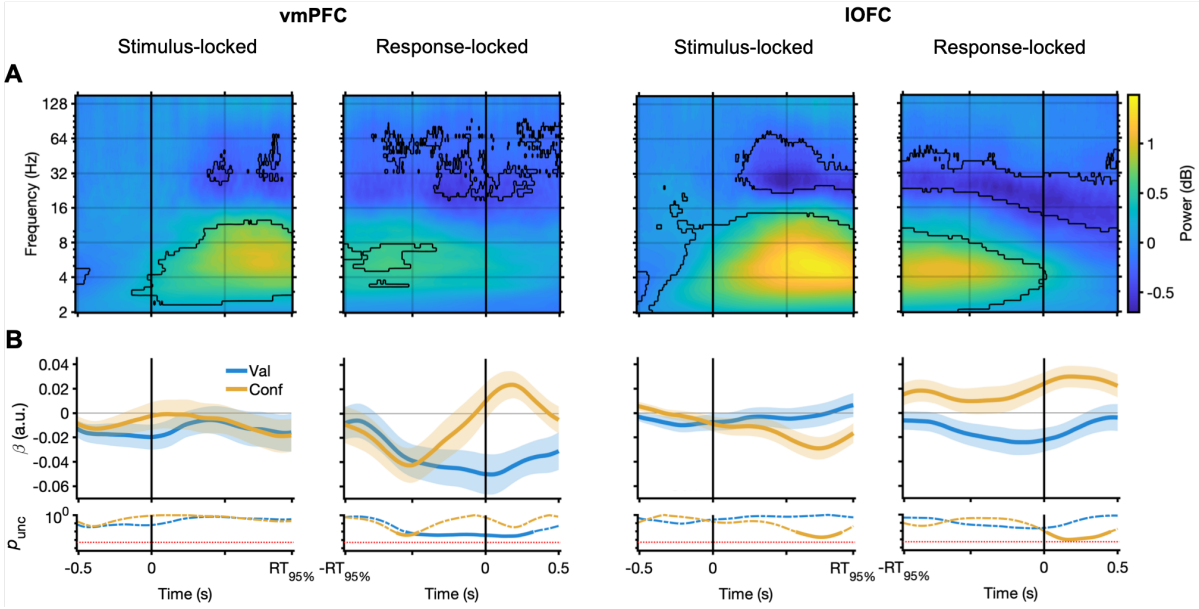

Figure 3-1. Val and Conf signals in vmPFC versus lOFC activity.

For each recording site located in either the vmPFC (n = 66, *left panels*) or the lOFC (n = 138, *right panels*), trial-by-trial iEEG time series were locked either to stimulus onset or button press. Vertical dotted lines indicate the time at which choice is still ongoing in 95% of trials ($RT_{95\%}$). The same analysis was applied to each site and results were then averaged across sites.

A) Time-frequency decomposition of the evoked response. Power at each frequency is corrected for baseline activity (mean over a 1-s pre-stimulus time window). Contour lines indicate significant clusters surviving Bonferroni correction.

B) Time course of Val and Conf regression estimates and significance levels. At each time point, power in the θ range (4-8 Hz) was regressed against Val and Conf. Significance level (uncorrected p-value) is estimated using a t-test of regression estimates

against zero, across recording sites. Horizontal red dotted lines indicate the Bonferroni-corrected statistical threshold; p-values are highlighted in bold when they survive correction based on random-field theory (RFT).

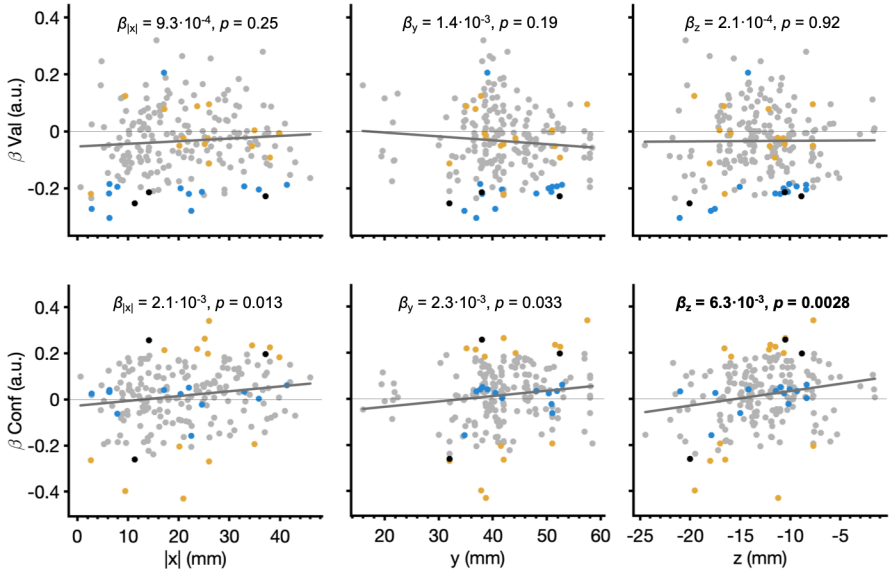

Figure 5-1. Spatial gradients of Val and Conf signals.

Spatial gradients of Val and Conf regression coefficients (top and bottom rows, respectively) were tested within the OFC along the medial-lateral (|x|), the posterior-anterior (y), and the caudal-rostral (z) axes (*left*, *middle*, and *right columns*, respectively). For each recording site, β regression coefficients were estimated across trials from a GLM fitted to the mean signal in the θ range (4-8 Hz), extracted from the [–0.5 s, 0.5 s] time window surrounding choice (button press). Then, the gradients were estimated using linear regressions of β estimates against MNI coordinates, separately for each of the three axes. Dots are recording sites; colors indicate significant associations (with Val in blue, with Conf in orange, with both in black); dark grey lines show the linear fits. Bold regression coefficient and p-value indicates the only significant gradient surviving Bonferroni correction (Conf signal along the z-axis).